PHYSICS AND CHEMISTRY OF SOLID STATE
V. 24, No. 4 (2023) pp. 595-602
Section: Physics

DOI: 10.15330/pcss.24.4.595-602

Vasyl Stefanyk Precarpathian National University

ФІЗИКА І ХІМІЯ ТВЕРДОГО ТІЛА
Т. 24, № 4 (2023) С. 595-602
Фізико-математичні науки

PACS:75.50.Gg; 63.50.-x

ISSN 1729-4428

Priyanka Kashid[1,3], S.N. Mathad[1,3], Mahadev R. Shedam[2]

Impact of Cd^{+2} substitutions on structural and mechanical properties of $Co_{0.6}Ni_{0.4-x}Cd_xFe_2O_4$ ($0.00 \leq x \leq 0.40$) system

[1]Department of Engineering Physics, K.L.E Institute of Technology, Hubballi, Karnataka, India,
physicssiddu@gmail.com, physicssiddu@kleit.ac.in
[2]Department of Physics, The New College, Kolhapur, India
[3]Visvesvaraya Technological University, Jnana Sangama, Belagavi, 590018, India

This article presents the structural and mechanical properties of $Co_{0,6}Ni_{0,4-x}Cd_xFe_2O_4$spinel ferrite nanoparticles. The as prepared samples were characterized by thermo-gravimetric differential thermal analysis to examine their phase transition. TGA/DTA analysis confirmed the reaction is endothermic in nature and the process completion temperature around 714.24oC is good for annealing the prepared ferrite powder. X-ray diffraction pattern revealed, $Co_{0,6}Ni_{0,4-x}Cd_xFe_2O_4$ have been well crystallized to spinel crystal structure. The average crystallite size ranging from 14.52nm to 16.92nm. FTIR spectra showed, two significant absorption bands (ν_1 and ν_2) in between 400 $cm^{-1}$and 600 cm^{-1}confirmed the spinel structured ferrites. Morphological observations revealed, the grain size of prepared ferrites lies in the range 0.85 to 0.21 μm. Raman spectra peak positions of both tetrahedral and octahedral sublattice shifted towards higher energy position.

Keywords: Co-precipitation method, Cobalt ferrite, Cd substitution, texture coefficients, vibrational modes, mechanical properties.

Received 18 May 2023; Accepted 26 September2023.

Introduction

The novel applications of nanoferrites in several fields have attracted researchers in their peculiar way of preparing these nanomaterials. The rapid development in synthesizing ferrite materials for new fields promises the major effect on lives of public and engineers in near future. Cobalt ferriteis a most attractive hard magnetic material with high crystalline anisotropy [1], moderate saturation magnetization [2], relatively high coercivity [3] and nickel ferrite is a soft magnetic material with low saturation magnetization [4], large expansion coefficient and low coercivity [5]. The combination of such hard and soft magnetic materials make them excellent in variety of applications.

Like other nanocomposites, the most interesting factor about cobalt nickel ferrite is their excellent properties with huge applications. In Cd substituted Co-Ni ferrite, dc resistivity at different sintering temperatures (1100ºC,1150ºC,1200ºC) decreased with increase of Cd content as reported [6]. The FTIR spectra of Cd substituted Ni-Zn ferrite confirmed the formation of spinel structure as investigated [7]. The effect of dysprosium on electrical and magnetic properties of Co-Ni ferrite was studied and saturation magnetization decreased with increase ofDy content as found [8]. In Ni-Cd ferrites, the structural properties and magnetic parameters are strongly dependent on Cd content as investigated [9].Bi substituted Co-Ni ferrite nanoparticles were hydrothermally prepared with formation of mono phase cubic spinel structure as explored [10]. Cation distribution of cadmium doped Ni-Zn ferrite at both tetrahedral and octahedral sites as observed [11]. The different ferrite nanocomposites were fabricated by some novel techniques likesolid state method [12], sol-gel method [13], double sintering ceramic method [14], hydrothermal method [15], sol-gel auto combustion method [16], ceramic method [17], coprecipitation method [18] and ball milling method [19].

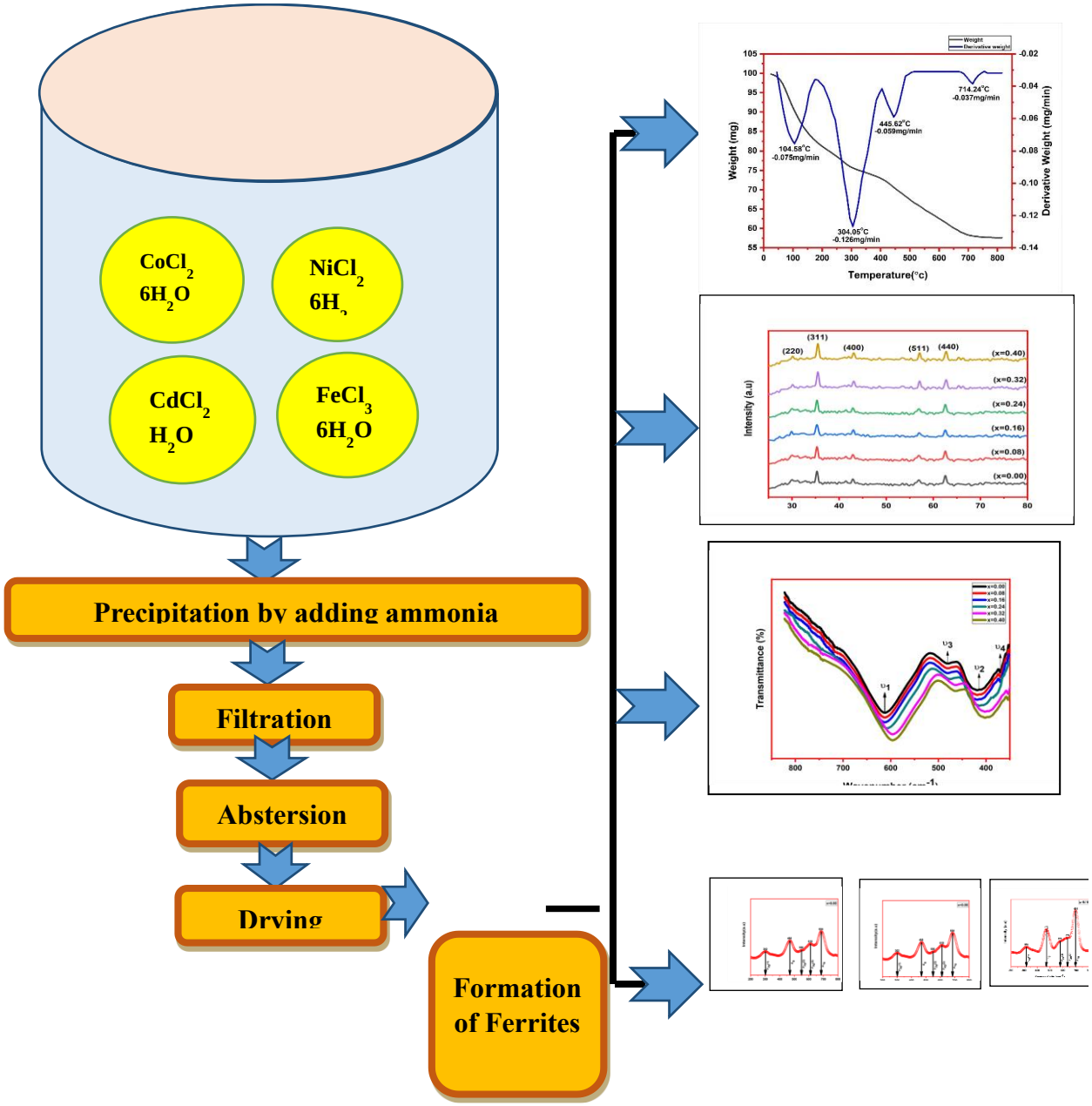

Fig. 1. Graphical abstract of $Co_{0.6}Ni_{0.4-x}Cd_xFe_2O_4$.

In this article, we established the synthesis and structural properties of Cd substituted Co-Ni ferrite. The prepared ferrite samples were synthesized by using the simple and cost effective co-precipitation technique. This preparation route shows remarkable advantages over the other preparation routes of ferrite nanoparticles such as low cost, simplicity [20], high product purity [21], specially water soluble nanoparticles directly obtained from this process. The results are subjected that the substitution of Cd into Co-Ni ferrite enhanced the structural and morphological properties of prepared ferrite nanoparticles.

I. Experimental Section

1.1. Synthesis

$Co_{0.6}Ni_{0.4-x}Cd_xFe_2O_4$ nanoparticles were systematically and successfullysynthesized through co-precipitation method. The high purity precursors such as cobalt chloride hexahydrate ($CoCl_2.6H_2O$), Nickel chloride hexahydrate ($NiCl_2.6H_2O$), cadmium chloride monohydrate ($CdCl_2.H_2O$), Ferric chloride hexahydrate ($FeCl_3.6H_2O$) and sodium hydroxide (NaOH) as precipitate agent were directly used for synthesis process. In a typical experiment, all chemical reactants were dissolved in 100 mL of distilled water and mixed with continuous stirring for 30 minutes at 60°C. Sodium hydroxide solution was added dropwise into the prepared mixture solution till a pH reached close to 8. During this synthesis, controlled size nanoparticles were obtained by controlling the nucleation and growth rates. The resulting brown color precipitate solution was washed by using distilled water and centrifuged at 2000 rpm. Then the precipitate was dried at room temperature for 3 days and was finely powdered in a clean agate mortar. Finally, the end product was sintered at 800°C in a muffle furnace for about 4 hours.

1.2. Characterizations

To investigate an idea about optimum sintering temperature, the prepared samples were characterized by using Thermogravimetric/Differential thermal analyzer system- SDT Q600. The Bruker AXS D8 Advance diffractometer was used to identify the structure of prepared ferrite samples and data was collected at diffraction angles (2θ) between 20^0 – 80^0. The Fourier transform infrared spectra of all samples were recorded using Thermo Nicolet, Avatar 370 FTIR spectrometer. The morphological images were captured on tungsten source based JEOL JSM-IT200 scanning electron microscope. Raman spectra of prepared samples were obtained on Bruker company's Senterra spectrometer.

II. Results and Discussion

2.1. Thermogravimetric analysis

In order to study the thermal behavior of $Co_{0.6}Ni_{0.4-x}Cd_xFe_2O_4$, thermogravimetric measurements of prepared ferrite powder was carried out in oxidizing atmosphere with flow rate of 10^0C/min. The TGA and DTA curves of an un-annealed compound are shown in figure 2. As indicated, the figure shows four weight losses are occurred within the temperature range of 50 -750ºC. The initial weight loss is occurred between room temperature and 175ºC, as shown by the very first DTA peak centered at 104.58ºC, is due to the removal of moisture in the residue. The second weight loss is occurred between 175ºC and 404ºC temperature, as shown by the DTA peak centered at 304.05ºC, is due to the breaking of coordination bond between water molecule and metal chlorides. The third weight loss is occurred between 404ºC and 486ºC temperature, as shown by the DTA curve centered at 445.62ºC, is due to the decomposition of remaining chloride precursors while the last weight loss occurred at 714.24ºC, attributed to crystallization of self combusted end product. Finally, no weight loss is occurred above 714.24ºC. From TGA/DTA results we concluded that, an optimal temperature of 714.24ºC is good for sintering the prepared ferrite samples. Thus for further characterizations, we were sintered all the samples at 800ºC for 4hrs.

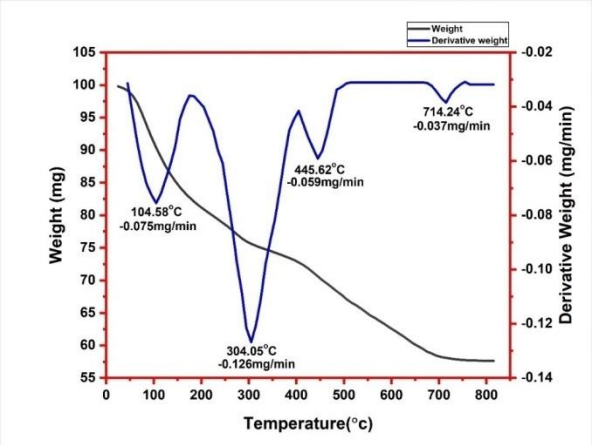

Fig. 2. TGA/DTA curves of $Co_{0.6}Ni_{0.32}Cd_{0.08}Fe_2O_4$ ferrite material.

2.2. XRD analysis

Figure 3, depicts the X-ray diffraction patterns for $Co_{0.6}Ni_{0.4-x}Cd_xFe_2O_4$ (x=0.00,0.08,0.16,0.24,0.32,0.40) system sintered at 800ºC for 4 hours. All existed peaks in XRD spectra were matched correctly with the standard system (JCPDS#00-22-1086) and therefore indicating the presence of single phase cubic spinel structure ferrite nanoparticles. Table 1. includes the structural parameters like crystallite size (D), lattice parameter (a), volume of unit cell (V), hopping length (L_A and L_B), bond length (A-O and B-O) and stacking fault coefficient (α) are calculated from the XRD measurements using following equations.

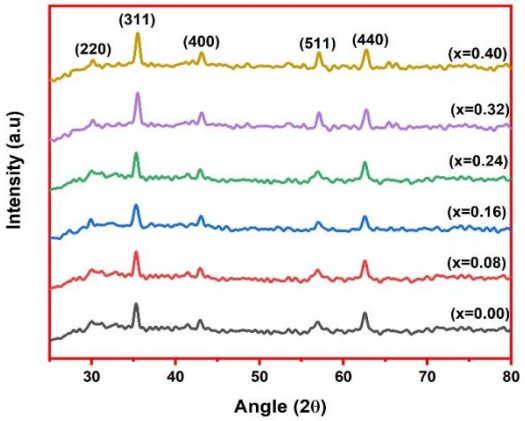

Fig. 3. Powder X-ray diffraction patterns for Cd doped Co-Ni spinel ferrite samples.

$$D = \frac{K\lambda}{\beta cos\theta} \quad (1)$$

Where D is the crystallite size, *K* is shape factor, λ is the X-ray wavelength (1.5406), β is the pure diffraction broadening and θ is the Bragg's diffraction angle.

$$\alpha = d_{hkl}\sqrt{h^2 + k^2 + l^2} \quad (2)$$

Where a is lattice constant, d is interplaner spacing with *hkl* are Miller indices. The volume ofunit cell is calculated by using equations (3).

$$V_{unitcell} = \alpha^3 \quad (3)$$

The hopping lengths (L_A and L_B) and bond lengths (A-O and B-O) aredetermined by using equation (4) to equation (7).

$$L_A = \frac{\alpha\sqrt{3}}{4} \quad (4)$$

$$L_B = \frac{\alpha\sqrt{2}}{4} \quad (5)$$

And

$$A - O = \left[u - \frac{1}{4}\right]\alpha\sqrt{3} \quad (6)$$

$$B - O = \left[\frac{5}{8} - u\right]\alpha \quad (7)$$

Where L_A and L_B indicates the distance (hopping

length) between magnetic ions at A site and B site respectively. A-O and B-O represents the bond lengths for tetrahedral and octahedral sites respectively with u is the oxygen ion parameter. Stacking fault coefficient (α) is calculated by using following equation.

$$\alpha = \frac{2\pi^2}{45\sqrt{3}} \frac{\Delta 2\theta}{tan\theta_{hkl}} \quad (8)$$

Where Δ2θ is the difference between standard and observed 2θ values.

From table 1. it is clear that, the average crystallite size of all samples is vary between 14.52 to 16.92 nm. The lattice parameter a, slightly increases with increase of Cd content. This increase of lattice constant obeying Vegard's law [22]. As is well known, the ionic radius of Cd^{2+} (1.03Å) is bigger than that of Ni^{2+} (0.63Å) thus lattice expansion occurs if $Ni^{2+}$is replaced with Cd^{2+}. This lattice expansion results in an increase of lattice constant with increasing x. The cell volume also increases with cadmium substitution. Both hopping lengths and bond lengths are increases with increase of Cd concentration. This behavior of both is similar to that revealed in literature [23]. Stacking fault analysis indicates the peaks existed in XRD pattern are in expected position and no unwanted dominant peak is observed. As shown in Table 1, Stacking fault coefficient shows vary small value. Texture coefficient gives the quantitative information of spatial crystal orientationwithin the material [24]. Such degree of orientation for each diffraction peak is calculated by using their intensities.

$$TC_{hkl} = \frac{\frac{I_{hkl}}{Io_{hkl}}}{\frac{1}{N}\sum\frac{I_{hkl}}{Io_{hkl}}} \quad (9)$$

Where$I_{(hkl)}$ and $I_{o(hkl)}$ stand for observed and standard intensities, N is the number of reflections existed in XRD pattern. The texture coefficient (TC) is higher than one shows preferential orientation and also shows abundance of grains along the given *hkl* plane. The calculated values of texture coefficient, TC are presented in Table 2. It is clear from Table 2, the values of TC (400) are higher than the others show higher orientation of crystallites occurs along these particular planes.

2.3. FTIR analysis

ThFFTIR spectra of Cd substituted Co-Ni ferrite nanoparticles are as shown in figure 4. FTIR spectra show two major peaks at (592-612) cm^{-1} and (398-416) cm^{-1} are in good agreement with the IR characteristics of spinel ferrites. However, for spinels, the high frequency band around 600 cm^{-1} attributes to tetrahedral (A) site and the low frequency band around 400 cm^{-1} corresponds to the octahedral (B) site [25]. Therefore, the existence of these two vibrational bands (ν_1) and (ν_2) confirm the spinel structure of prepared ferrite nanoparticles. The values of vibrational bands of $Co_{0.6}Ni_{0.4-x}Cd_xFe_2O_4$ samples are listed in Table 3. As indicated, table 3 exhibits these vibrational bands shift towards lower frequencies with increase of Cd content, this is due to the increase in lattice parameter with increase of Cd content as discussed in XRD analysis [26]. According to Waldron [27],

Table 1.

The calculated values of crystallite size, lattice constant, cell volume, hopping length,bond length and stacking fault coefficient of$Co_{0.6}Ni_{0.4-x}Cd_xFe_2O_4$.

Parameters	x=0.00	x=0.08	x=0.16	x=0.24	x=0.32	x=0.40
Crystallite size 'D' (nm)	16.92	14.52	15.67	14.56	15.71	14.70
Lattice constant 'a' (Å)	8.4004	8.4052	8.4141	8.4259	8.4324	8.4387
$V_{unit\ cell}$ ($Å^3$)	592	593	595	598	599	600
Hopping length 'L_A'(Å)	3.6375	3.6396	3.6434	3.6485	3.6513	3.6541
Hopping length 'L_B'(Å)	2.970	2.9717	2.9748	2.9790	2.9813	2.9835
Bond length 'A-O'(Å)	1.8187	1.8198	1.8217	1.8243	1.8257	1.8270
Bond length'B-O'(Å)	2.1001	2.1013	2.1035	2.1065	2.1081	2.1097
Stacking fault coefficient 'α'	0.001012	0.001218	0.001544	0.002279	0.002708	0.003088

Table 2.

Texture coefficient values for different *hkl* planes

hkl	x=0.00	x=0.08	x=0.16	x=0.24	x=0.32	x=0.40
220	1.1413	1.2341	1.2896	1.2756	1.2582	1.2785
311	0.4654	0.4352	0.4214	0.4197	0.4170	0.4166
400	1.7453	1.8686	1.9469	1.9355	1.9459	1.9569
511	1.1191	1.2283	1.2608	1.2840	1.3415	1.3087
440	1.0056	1.0046	0.9858	1.0004	0.9840	0.9905

Table 3.

Band positions of IR peaks for Cd doped Co-Ni ferrites

x	0.00	0.08	0.16	0.24	0.32	0.40
$\nu_1(cm^{-1})$	612	611	610	606	595	592
$\nu_2(cm^{-1})$	416	413	412	411	400	398
$\nu_3(cm^{-1})$	482	481	479	477	464	462
$\nu_4(cm^{-1})$	370	369	368	361	353	351

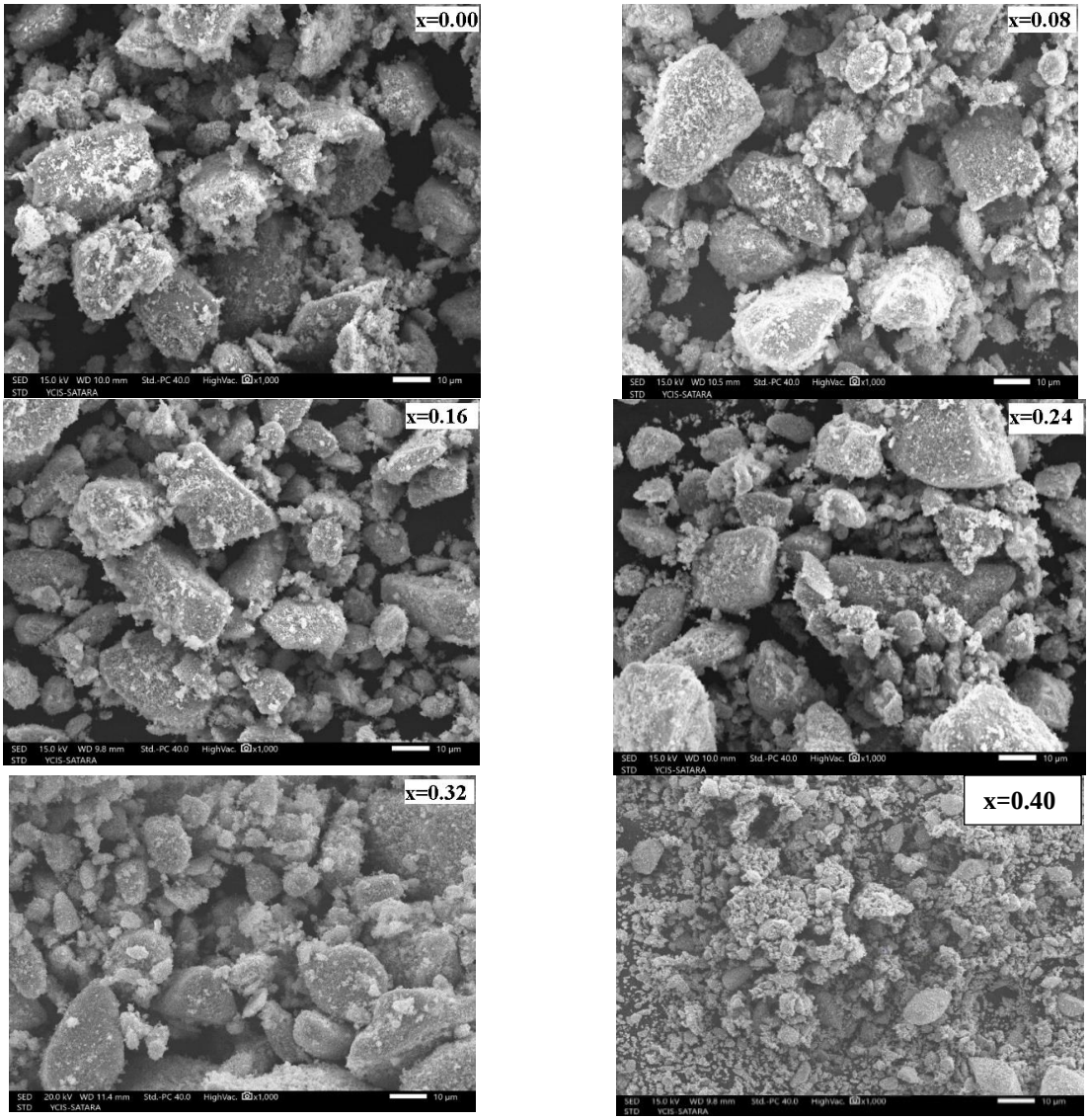

Fig. 5.SEM images for $Co_{0.6}Ni_{0.4-x}Cd_xFe_2O_4$ samples.

$\nu_1$peakattributes to the intrinsic stretching vibration of tetrahedral site andν_2 corresponds to stretching vibration of M-O bond in octahedral site. The 3rd peak $\nu_3$and 4th peakν_4 attributes to vibration of metal and oxygen ions in isotropic force field of their octahedral and tetrahedral sites respectively. Similar splitting of IR absorption bands was reported in literature [28].

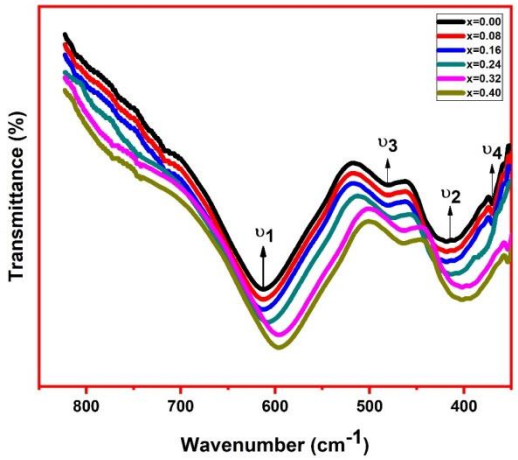

Fig. 4. FTIR spectra of $Co_{0.6}Ni_{0.4-x}Cd_xFe_2O_4$ ferrite samples.

2.4. SEM analysis

To obtain an accurate details of the morphology and microstructure of ferrite nanoparticles, SEM has been performed. The SEM images of $Co_{0.6}Ni_{0.4-x}Cd_xFe_2O_4$ nanoparticles as shown in figure 5. All the samples show a tendency towards agglomeration due to Van-der Wall weak force arising between the particles as well as magnetic nature of the sample, revealing the formation of spherical/rock shaped ferrite nanoparticles. Based on SEM micrographs, the average grain size was found to be in the range of 0.85 to 0.21 μm. This decrease is due to greater ionic radius of dopant (Cd^{2+}). Cd^{2+} ions because of its greater size when diffuse into the nickel ferrite grains, create more residual stress, revealing the formation of smaller sized grains. The average crystallite sizes of ferrite nanoparticles determined by XRD are considerably smaller in comparison to that achieved by SEM images [29].

2.5. Raman analysis

Further to obtain the structural properties of prepared ferrite samples Raman spectroscopy has been performed. Raman spectra of Cd doped Co-Ni ferrite is as shown in

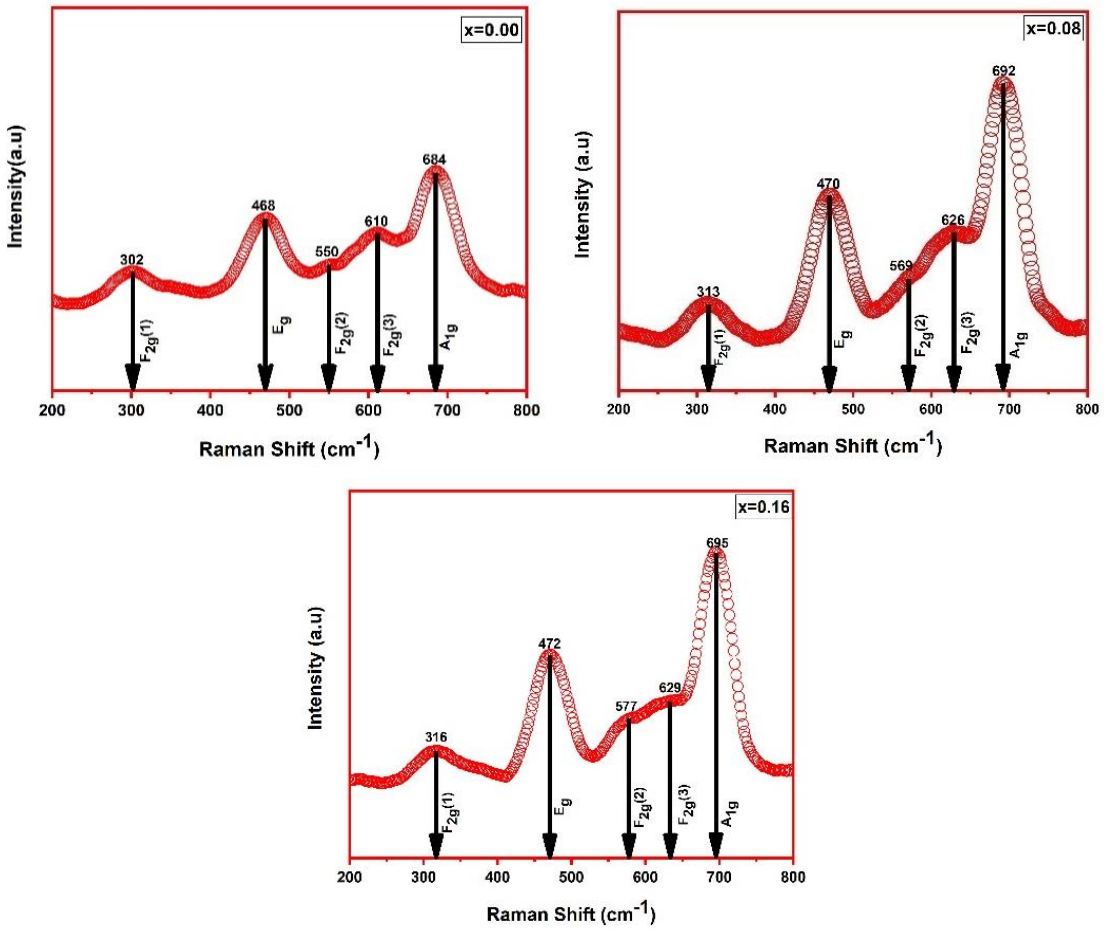

Fig.6. Raman spectra of Cd doped CoNi ferrite nanoparticles.

Table 4.

Raman peaks for $Co_{0.6}Ni_{0.4-x}Cd_xFe_2O_4$ series with x=0.00,0.08,0.16

Conc. x	$A_{1g}(1)$ cm-1	$F_{2g}(3)$ cm-1	$F_{2g}(2)$ cm-1	$E_g$cm-1	$F_{2g}(1)$ cm-1
0.00	684	610	550	468	302
0.08	692	626	569	470	313
0.16	695	629	577	472	316

Figure 6. The group theory analysis predicts the following five Raman active modes are easily fitted in spinel [30,31].

$$A_{1g} + E_g + 3F_{2g}$$

Where, A_{1g} Raman mode corresponds to symmetric stretching of oxygen atom with respect to metal ion in tetrahedral sublattice. The E_g Raman mode associates to symmetric bending of oxygen atom with respect to metal ion in octahedral sublattice. The $F_{2g}(2)$ and$F_{2g}(3)$ modes correspondto asymmetric stretching and asymmetric bending at octahedral sublattice respectively.Further, $F_{2g}(1)$ Raman mode corresponds to translation movement of four oxygen atoms with metal ion in tetrahedral sublattice. All existed Raman active modes are presented in table 4, and are in good agreement with the previous reports [31,32]. In spinel ferrites, the frequency modes above 600cm^{-1} are assigned to motion of oxygen atom in tetrahedral sublattice whereas the modes below this frequency correspond to the vibrations of oxygen atoms in octahedral sites. It can be seen from figure 6, for the most intense peak [$A_{1g}(1)$], a clear increase in intensity can be seen with an increase of cadmium substitution. All vibrational modes shift towards higher energy positions due to cation distribution between tetrahedral and octahedral sites [31,32].

Conclusion

The aim of this article was to enhance the properties of Co-Ni nano-ferrites with Cd substitution. In this summary, the effect of cadmium on structural, microstructural, Infra-red and Raman properties of $CoNiFe_2O_4$ synthesized by co-precipitation method has been explored. The following important conclusions were found through present study:

The obtained ferrite samples were annealed at 800ºC, such temperature that was found using TGA/DTA analysis.

In the XRD data, we concluded that the lattice parameters increased slightly with increase of dopant concentration. Texture coefficient analysis shows the abundance of (400) plane for preferential orientation.

FTIR and Raman spectroscopies affirmed the

presence of bonds correspond to the spinel structure.

The average crystallite size and grain size of all prepared ferrites are lies in nano and micro particle range, verifies the formation of nanoferrites.

Kashid Priyanka –M.Sc., Ph.D. scholar, Department of Engineeing Physics, K.L.E. Institute of Technology, Visvesvaraya Technological University, Jnana Sangama, Belagavi, 590018, India;
Mathad S.N.– M.Sc., Ph.D., Head of the Department, Department of Engineering Physics, K.L.E. Institute of Technology, Hubballi, Supervisor;
ShedamMahadev R. – M.Sc., Ph.D., Head of Department of Physics.

[1] S.I. Ahmad, *Nano cobalt ferrites: Doping, Structural, Low-temperature, and room temperature magnetic and dielectric properties – A comprehensive review*, J. Magn. Magn. Mater., 562, 169840 (2022); https://doi.org/10.1016/j.jmmm.2022.169840.
[2] S. Rasheed, R.Ali Khan, F.Shah, A.Rahim, A.R.Khan, *Enhancement of electrical and magnetic properties of cobalt ferrite nanoparticles by co-substitution of Li-Cd ions*, J. Magn. Magn. Mater., 471, 236 (2019); https://doi.org/10.1016/j.jmmm.2018.09.073.
[3] S. Jauhar, J. Kaur, A. Goyal, S. Singhal, *Tuning the properties of cobalt Ferrite: A road towards diverse applications*,RSC Advances. 6, 97694 (2016); https://doi.org/10.1039/C6RA21224G.
[4] K. Nejatiand, R. Zabihi, *Preparation and magnetic properties of nano size nickel ferrite particles using hydrothermal method*,Chem Cent J., 6, 23 (2012).
[5] A.S. Molakeri, S. Kalyane, A.B. Kulkarni, S.N. Mathad, *Elastic Properties of Nickel Ferrite Synthesized by Combustion and Microwave Method using FT-IR Spectra*, Int. J. Adv. Sci. Eng., 3 (4), 422 (2017).
[6] M.A. Hakim, S.K.Nath, S.S.Sikder,K.H.Maria, *Cation distribution and electromagnetic properties of spinel type Ni–Cd ferrites*,J. Phys. Chem. Solids, 74 (9), 1316 (2013); https://doi.org/10.1016/j.jpcs.2013.04.011.
[7] M.R. Patil, M. K. Rendale, S. N. Mathad and R. B. Pujar, *Electrical and magnetic properties of Cd^{+2} doped Ni-Zn ferrites*, J. Inorganic and Nano-Metal Chemistry, 47(8), 1145 (2017);https://doi.org/10.1080/24701556.2017.1284097.
[8] A.A. Kadam, S.S.Shinde, S.P.Yadav, P.S.Patil, K.Y.Rajpure, *Structural, morphological, electrical and magnetic properties of Dy doped Ni–Co substitutional spinel ferrite*, J. Magn. Magn. Mater.,329, 59 (2013); https://doi.org/10.1016/j.jmmm.2012.10.008.
[9] M.Rahimi, M. Eshraghi, P. Kameli, *Structural and magnetic characterizations of Cd substituted nickel ferrite nanoparticles*, Ceram. Inter.4 (10),15569 (2014); https://doi.org/10.1016/j.ceramint.2014.07.033.
[10] A.N. Alquarni, M.A. Almessiere, S. Guner, M. Sertkol, S.E. Shirsath, N. Tashkandi, A.Baykal, *Structural and magnetic properties of hydrothermally synthesized Bi-substituted Ni–Co nanosized spinel ferrites*,Ceram. Inter. 48, 5450 (2022); https://doi.org/10.1016/j.ceramint.2021.11.089.
[11] P.A.Rao, V.Raghavendra, B.Suryanarayana, T.Paulos, N.Murali, P.V.S.K.Phanidhar Varma, R.Giri Prasad, Y.Ramakrishna, K.Chandramouli, *Cadmium substitution effect on structural, electrical and magnetic properties of Ni-Zn nano ferrites*, Results Phys. 19, 103487 (2020); https://doi.org/10.1016/j.rinp.2020.103487.
[12] S. N. Mathad, R. N. Jadhav and Vijaya Puri, *Raman studies of Rod-like Bismuth strontium manganites*, Euro. J. Appl. Eng. Sci. Res., 1(3),67 (2012).
[13] Dong-Hwang Chen, Xin-Rong He, *Synthesis of nickel ferrite nanoparticles by sol-gel method*, Mater. Res. Bul., 36(7-8), 1369 (2001); https://doi.org/10.1016/S0025-5408(01)00620-1.
[14] S. S. Bellad,S. C. Watawe, A. M. Shaikh&B. K. Chougule, *Cadmium substituted high permeability lithium ferrite*, Bull. Mater. Sci., 23, 83 (2000); https://doi.org/10.1007/BF02706546.
[15] C.Tsay, Y.Chiu, C. Lei,*Hydrothermally Synthesized Mg-Based Spinel Nanoferrites: Phase Formation and Study on Magnetic Features and Microwave Characteristics*, Materials 11, 2274 (2018); https://doi.org/10.3390/ma11112274.
[16] S.A. Mhamad, A.A.Ali, S.S.Mohtar, F.Aziz, M.Aziz, J.Jaafar, N.Yusof, W.Salleh, A.Ismail, S.Chandren,*Synthesis of bismuth ferrite by sol-gel auto combustion method: Impact of citric acid concentration on its physicochemical properties*, Mater. Chem. Phys., 282, 125983 (2022); https://doi.org/10.1016/j.matchemphys.2022.125983
[17] L. Agusu, M. Firihu, S.Mitsudo, H.Kikuchi, *Crystal and microstructure of MnFe2O4 synthesized by ceramic method using manganese ore and iron sand as raw materials*, J. Phys.: Conf. Ser., 1153(1), 012056 (2019); https://doi.org/10.1088/1742-6596/1153/1/012056.
[18] B.B. Patil, A.D. Pawar, D.B. Bhosale, J.S. Ghodake, J.B. Thorat, TJ Shinde, *Effect of La^{3+} substitution on structural and magnetic parameters of Ni–Cu–Zn nano-ferrites*, J. nanostructure chem., 9(2), 119 (2019); https://doi.org/10.1007/s40097-019-0302-0.
[19] R.Turtelli, M.Atif, N.Mehmood, F.Kubel, K.Biernacka, W.Linert, R.Grossinger, Cz.Kapusta, M.Sikora, *Interplay between the cation distribution and production methods in cobalt ferrite*, Mater. Chem.Phys., 132, 832 (2012); https://doi.org/10.1016/j.matchemphys.2011.12.020.

[20] R.M. Shedam, A.B. Gadkari, S.N. Mathad, M. R. Shedam, *Structural and mechanical properties of nanograined magnesium ferrite produced by oxalate coprecipitation method*, Int. J. Self-Propagating High-Temp. Synth., 26(1), 75 (2017); https://doi.org/10.3103/S1061386217010113.

[21] S. Irfan, M. Nabi, Y. Jamil, N.Amin, *Synthesis of $Mn_{1-x}Zn_xFe_2O_4$ ferrite powder by co-precipitation method*, Mater. Sci. Eng., 60, 012048 (2014); https://doi.org/10.1088/1757-899X/60/1/012048.

[22] S.M. Patange, S.E. Shirsath,B.G. Toksha,S.S. Jadhav, K.M. Jadhav, *Electrical and magnetic properties of Cr^{3+}substituted nanocrystalline nickel ferrite*, J. Appl. Phys., 106(2), 023914 (2009); https://doi.org/10.1063/1.3176504.

[23] A.B. Kulkarni, S. N. Mathad, *Effect of cadmium doping on structural and magnetic studies of Co-Ni ferrites*, Sci. Sinter., 53 (3), 407 (2021); https://doi.org/10.2298/SOS2103407K.

[24] H.R.Shashidhargouda, S.N.Mathad, *Synthesis and structural analysis of $Ni_{0.45}Cu_{0.55}Mn_2O_4$ by Williamson–Hall and size–strain plot methods*, Ovidius Univ. Ann. Chem., 29(2), 122 (2018); https://doi.org/10.2478/auoc-2018-0018.

[25] J.Massoudi, M.Smari, K. Nouri, E.Dhahri, K.Khirouni, S. Bertaina, L.Bessais, El.Hlil, *Magnetic and spectroscopic properties of Ni–Zn– Al ferrite spinel: from the nanoscale to microscale*, RSC Adv. 10, 34556 (2020); https://doi.org/10.1039/D0RA05522K.

[26] S.A.Patil, S.M.Otari, V.C.Mahajan, M.G.Patil, A.B.Patil, M.K.Soudagar, B.L.Patil, S.R.Sawant, *Structural, IR and magnetisation studies on La^{3+} substituted copper ferrite*, Solid State Commun., 78 (1), 39(1991); https://doi.org/10.1016/0038-1098(91)90805-6.

[27] R.D. Waldron, *Infrared Spectra of Ferrites*, Physical Review, 99, 1727 (1955); https://doi.org/10.1103/PhysRev.99.1727.

[28] M.R. Patil, M.K. Rendale, S.N. Mathad, R.B. Pujar, *Structural and IR study of $Ni_{0.5-x}Cd_xZn_{0.5}Fe_2O_4$,* Int., J. Self-Propag. High Temp. Synth., 24, 241 (2015); https://doi.org/10.3103/S1061386215040081.

[29] R.Vishwarup, S.N.Mathad, *Elastic properties of nano $Mg_{1-x}Co_xFe_2O_4$ (x= 0.15, 0.2, 0.25, 0.3, 0.35 and 0.4) synthesized by co-precipitation method*, J. Mater. Sci. Energy Technol., 3, 559 (2020); https://doi.org/10.1016/j.mset.2020.05.006.

[30] G.M. Shweta, L. R. Naik, R.B. Pujar, S.N. Mathad, *Influence of Magnesium doping on structural and elastic parameters of Nickel Zinc nanoferrites*, Materials Chemistry and Physics, 257(1), 123825 (2021); https://doi.org/10.1016/j.matchemphys.2020.123825.

[31] G.M. Shweta, L.R. Naik, R.B. Pujar, S.N.Mathad, *Cobalt-Doped Nickel Zinc Nanoferrites by Solution-Combustion Synthesis: Structural and Elastic Parameters*, Int. J Self-Propag. High-Temp. Synth. 29, 157 (2020); https://doi.org/10.3103/S1061386220030115.

[32] D. Bouokkeze, J. Massoudi, W. Hzez, M. Smari, A. Bougoffa, K. Khirouni, E. Dhahri, L. Bessais,*Investigation of the structural, optical, elastic and electrical properties of spinel $LiZn_2Fe_3O_8$ nanoparticles annealed at two distinct temperatures*, RSC Adv., 9. 40940 (2019); https://doi.org/10.1039/C9RA07569K.

П.П. Кашид[1], Ш.Н. Матад[1], М.Р. Шедам[2]

Вплив заміщенняCd+[2] на структурно-механічні властивості системи $Co_{0,6}Ni_{0,4-x}Cd_xFe_2O_4$ (0,00 ≤ x ≤ 0,40)

[1]Кафедра фізики, Технологічний інститут Товариства K.L.E, Хублі, Індія,physicssiddu@gmail.com, physicssiddu@kleit.ac.in
[2]Кафедра фізики, Новий коледж, Колхапур, Індія;
[3]Технологічний університет Вісвесварая, Джнана Сангама, Белагаві, Індія

У статті наведено структурно-механічні властивості феритових наночастинок шпінелі $Co_{0,6}Ni_{0,4-x}Cd_xFe_2O_4$. Підготовлені зразки досліджували термогравіметричним диференціально-термічним аналізом з метою вивчення фазового переходу. Аналіз TGA/DTA підтвердив, що реакція має ендотермічний характер, і температура завершення процесу близька 714,24°C та є хорошою для відпалу підготовленого феритового порошку. Рентгенівський дифракційний аналіз показав, що $Co_{0,6}Ni_{0,4-x}Cd_xFe_2O_4$ кристалізовано у кристалічній структурі шпінелі. Середній розмір кристалітів коливається від 14,52 нм до 16,92 нм. Спектри FTIR показали дві значні смуги поглинання (ν_1 і ν_2) між 400 $см^{-1}$ і 600 $см^{-1}$, що підтверджує наявність феритів зі структурою шпінелі. Морфологічні спостереження показали, що розмір зерна отриманих феритів знаходиться в діапазоні 0,85-0,21 мкм. Положення піків спектрів комбінаційного розсіювання як тетраедричної, так і октаедричної підграток зміщені в бік вищої енергетичної позиції.

Ключові слова: метод співосадження, ферит кобальту, заміщення Cd, текстурні коефіцієнти, коливальні моди, механічні властивості.